Journal of Inorganic Biochemistry 193 (2019) 42–51

Contents lists available at ScienceDirect

Journal of Inorganic Biochemistry

journal homepage: www.elsevier.com/locate/jinorgbio

Photoinduced electron transfer within supramolecular hemoprotein co-assemblies and heterodimers containing Fe and Zn porphyrins

Ryota Kajihara[a], Koji Oohora[a,b,c,*], Takashi Hayashi[a,**]

[a] Department of Applied Chemistry, Graduate School of Engineering, Osaka University, Suita 565-0871, Japan
[b] Frontier Research Base for Global Young Researchers, Graduate School of Engineering, Osaka University, Suita 565-0871, Japan
[c] PRESTO, Japan Science and Technology Agency (JST), Kawaguchi 332-0012, Japan

ARTICLE INFO

Keywords:
Photoinduced electron transfer
Hemoprotein assembly
Hydrogen bond network
Cytochrome b_{562}
Marcus theory

ABSTRACT

Electron transfer (ET) events occurring within metalloprotein complexes are among the most important classes of reactions in biological systems. This report describes a photoinduced electron transfer between Zn porphyrin and Fe porphyrin within a supramolecular cytochrome b_{562} (Cyt b_{562}) co-assembly or heterodimer with a well-defined rigid structure formed by a metalloporphyrin–heme pocket interaction and a hydrogen-bond network at the protein interface. The photoinduced charge separation (CS: k_{CS} = 320–600 s^{-1}) and subsequent charge recombination (CR: k_{CR} = 580–930 s^{-1}) were observed in both the Cyt b_{562} co-assembly and the heterodimer. In contrast, interestingly, no ET events were observed in a system comprised of a flexible and structurally-undefined co-assembly and heterodimers which lack the key hydrogen-bond interaction at the protein interface. Moreover, analysis of the kinetic constants of CS and CR of the heterodimer using the Marcus equation suggests that a single-step ET reaction occurs in the system. These findings provide strong support that the rigid hemoprotein-assembling system containing an appropriate hydrogen-bond network at the protein interface is essential for monitoring the ET reaction.

1. Introduction

The biochemical processes of respiration and photosynthesis both include numerous precise electron transfer (ET) processes mediated by many metalloproteins and cofactors [1–4]. It is of particular interest that proteins provide a suitable medium to achieve efficient ET reactions over distances as long as 15 Å because protein matrices provide efficient electronic coupling and low reorganization energy [3]. These long-range ET reactions via protein matrices are often found in natural protein complexes as well as artificially constructed systems containing two or more redox-active sites [2,3,5–10]. Generally, the kinetic constants of electron tunneling depend on the electron donor–acceptor distances [2,3,11,12]. The distance decay constant (β) of electron tunneling in a protein is usually within the range of 1.0–1.3 $Å^{-1}$ which is a much smaller range relative to tunneling ranges measured in aqueous solution. Long-range ET reactions with donor–acceptor distances > 25 Å in a protein are rare, with the exception of multistep electron hopping through intermediate redox-active aromatic residues (e.g. Trp, Tyr, Phe) [6–8] and/or other redox-active molecules [4,9]. Therefore, a single-step and long range ET reaction requires a suitable protein scaffold and/or an appropriate protein–protein interface to achieve efficient electronic coupling for an interprotein ET. Particularly, in the latter case, we recognized that an artificial metalloprotein complex or assembly would provide a useful tool to understand such long range ET processes within a unique protein–protein complex. Over the last two decades, functional modeling efforts using engineered metalloprotein complexes have been successful in elucidating the mechanisms of the ET events [13–17]. In this respect, recent investigations of artificial metalloprotein assemblies independently reported by several groups [18,19] are expected to contribute to the creation of new classes of ET systems. Most of these previous investigations employed supramolecular self-assemblies of protein units which were formed via coordination-bonding interactions to achieve thermodynamically stable assemblies containing metal ions as potent redox-active moieties [16,20–23]. However, demonstrations of ET events occurring within these metalloprotein assemblies have been quite limited thus far.

Hemoproteins are redox-active metalloproteins and represent attractive candidates for investigations of ET reactions because heme (Fe protoporphyrin IX, FeP) can act as a ubiquitous electron donor or acceptor. Our group has recently prepared supramolecular hemoprotein

* Correspondence to: K. Oohora, Frontier Research Base for Global Young Researchers, Graduate School of Engineering, Osaka University, Suita 565-0871, Japan.
** Corresponding author.
E-mail addresses: oohora@chem.eng.osaka-u.ac.jp (K. Oohora), thayashi@chem.eng.osaka-u.ac.jp (T. Hayashi).

https://doi.org/10.1016/j.jinorgbio.2019.01.001
Received 17 December 2018; Accepted 3 January 2019
Available online 14 January 2019
0162-0134/

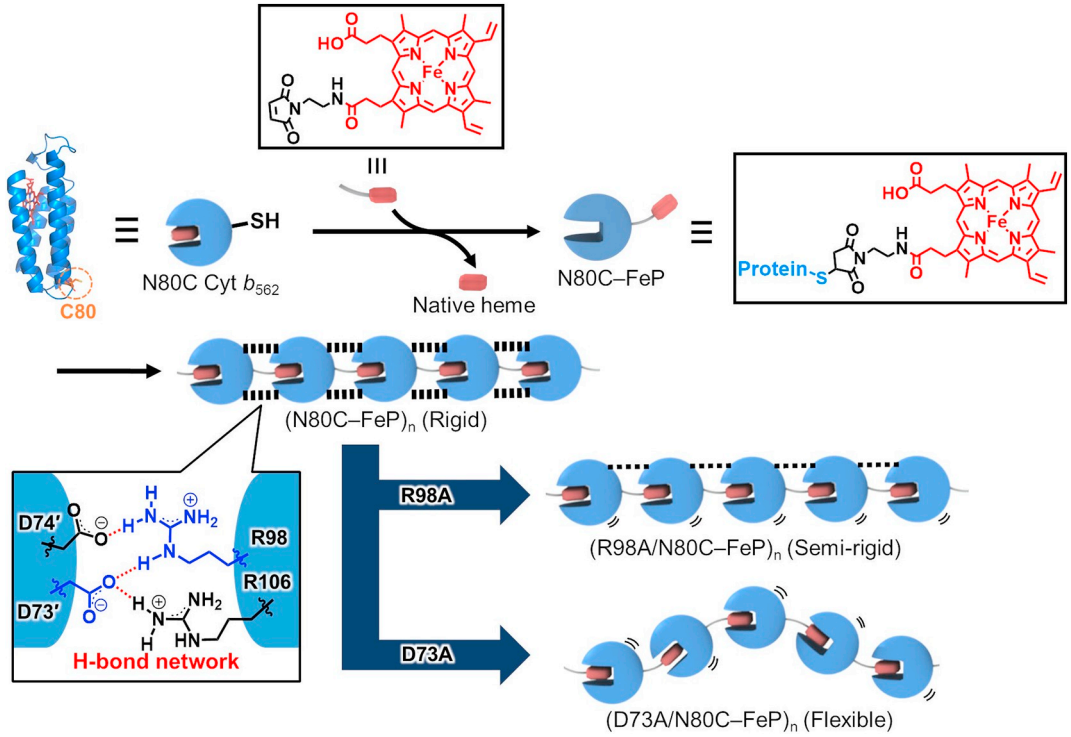

Fig. 1. Preparation of three Cyt b_{562} assemblies based on the Cyt b_{562} mutants N80C, R98A/N80C, and D73A/N80C.

assemblies where an iron protoporphyrin IX (FeP) analog is covalently attached to the surface of a monomeric hemoprotein unit [24,25]. In one previous example, FeP or zinc protoporphyrin IX (ZnP) with a maleimide moiety at one of the propionate side chains was linked to the engineered cysteine residue of the H63C mutant of cytochrome b_{562} (Cyt b_{562}) to generate an artificial cofactor-linked Cyt b_{562}. This engineered and modified hemoprotein enables us to provide Cyt b_{562} assemblies via the cofactor–heme pocket interaction [26–29] Since Cyt b_{562} is known to be an ET protein with a relatively simple structure formed by four α-helix bundles [30], the modified hemoprotein is expected to provide a potent building block for constructing ET models. Furthermore, we have recently prepared a Cyt b_{562} assembly using a single mutant, N80C, where the artificial metalloporphyrin is attached to the protein surface at the 80th residue [27]. This provides a structurally-defined assembly via the hydrogen-bond (H-bond) interaction between the protein interfaces as a secondary interaction (Fig. 1). The fibrous and periodic helical structure in solution was characterized by atomic force microscopy (AFM) measurements, indicating a helix with a 3-nm pitch. A circular dichroism (CD) spectrum of this protein shows a split-type Cotton effect in the range of 390–450 nm due to the fixed orientation of the FeP molecules. Confirmation of the fine structure was also supported by the results of a molecular dynamics (MD) simulation validated by mutation experiments. A mutant, D73A/N80C, was generated to provide a flexible assembly due to absence of the H-bond network between the proteins. The flexible nature of the D73A/N80C mutant assembly was confirmed by AFM and the absence of the split-type Cotton effect in the CD spectrum. Furthermore, the CD spectrum of the modified R98A/N80C assembly was found to exhibit an incomplete split-type Cotton effect, indicating that a semi-rigid (or semi-flexible) structure is provided by the weakened H-bond network (Fig. 1) [31]. Therefore, a series of three Cyt b_{562} assemblies with variable conformational flexibility is now available for ET studies.

Over the past two decades, several investigations of ET systems using Zn porphyrin have been conducted using synthetic molecules [32–36] and hemoprotein complexes [13–15,17,37–40]. In the latter case, Zn-substituted hemoprotein complexes have been investigated including: complexes of cytochrome *c*/Zn-substituted cytochrome *c* peroxidase, cytochrome b_5/Zn-substituted myoglobin, Zn-substituted α-hemoglobin, Zn-cofactor-reconstituted myoglobin/cytochrome *c*, and a co-crystal of cytochrome *c*/Zn-substituted cytochrome *c* where ferric heme is reduced by a photoexcited Zn porphyrin [13–15,17,37–39]. In contrast, in the present work, we report an investigation of photoinduced ET in the N80C-based Cyt b_{562} co-assemblies containing the FeP and the ZnP artificial cofactor on the proteins (Fig. 2a). Furthermore, the photoinduced ET events are also investigated in a simple system using six different N80C-based Cyt b_{562} heterodimers (Fe-Zn dimers and Zn-Fe dimers; Fig. 2b).

2. Experimental procedures

2.1. Materials and methods

ESI-TOF MS analyses were performed with a Bruker Daltonics micrOTOF II mass spectrometer. UV–vis spectra were measured with a Simadzu UV-3150 or UV-2550 double-beam spectrometer or JASCO V-670 spectrophotometer. Circular dichroism (CD) spectrum was recorded with a JASCO J-820S spectrometer. Luminescence spectra were measured with a JASCO FP-8600 fluorescence spectrometer. Size exclusion chromatographic (SEC) analyses were performed using an ÄKTApurifier system (GE Healthcare) at 4 °C. The pH measurements were carried out with an F-52 Horiba pH meter. Air-sensitive manipulations were performed in a UNILab glove box (MBraun, Germany). The equipment used for flash photolysis experiments is described below.

Iron and zinc protoporphyrin IX complexes (FeP, ZnP) with a maleimide group provided at the one of the propionate side chains via a linker molecule (m–FeP, m–ZnP) were prepared according to previous reports [28,29]. ZnP was synthesized using a conventional procedure [41]. FeP and other reagents and chemicals were purchased and used as received. Cytochrome b_{562} (Cyt b_{562}) and its mutants were expressed in the TG1 strain of *E. coli* and purified as previously reported [42]. Apoforms of the proteins (wild-type Cyt b_{562} (WT), N80C, R98A, and D73A/

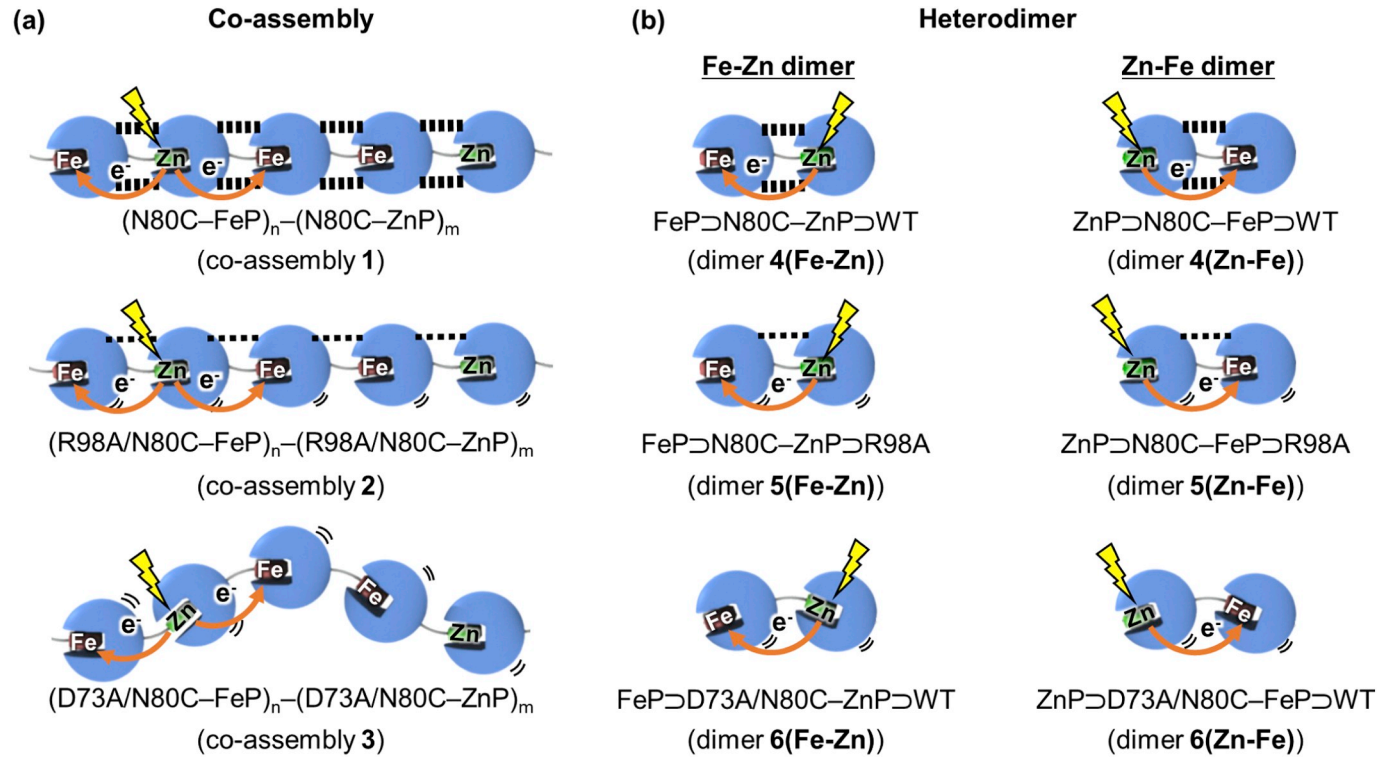

Fig. 2. Photoinduced ET in (a) three different Cyt b_{562} co-assemblies and (b) six different N80C-based Cyt b_{562} heterodimers (Fe-Zn dimers and Zn-Fe dimers).

N80C) were prepared by Teale's conventional 2-butanone method [43]. The Cyt b_{562} assemblies containing FeP ($(N80C–FeP)_n$, $(R98A/N80C–FeP)_n$, and $(D73A/N80C–FeP)_n$) were prepared as previously reported [27].

2.2. Preparation of cytochrome b_{562} co-assemblies

The N80C Cyt b_{562} co-assembly containing FeP and ZnP (co-assembly **1**, $(N80C–FeP)_n–(N80C–ZnP)_m$) was prepared by mixing the $(N80C–FeP)_n$ and $(N80C–ZnP)_m$ assembly (n/m = 1/1, 2/1, 3/1, [N80C–ZnP] = 3 μM) and allowing it to equilibrate for > 10 h under an N_2 atmosphere (Fig. 3a). The equilibration was confirmed by size exclusion chromatography using Superdex 200 10/300 GL (GE Healthcare). Other co-assemblies, co-assembly **2** and co-assembly **3**, were prepared according to the same procedures used to prepare co-assembly **1**.

2.3. Preparation of cytochrome b_{562} Fe-Zn heterodimers

Reconstituted wild-type Cyt b_{562} with maleimide-linked ZnP (m–ZnP ⊃ WT, 50 nmol) and N80C Cyt b_{562} (FeP ⊃ N80C, 150 nmol) were added to 4 mL of 100 mM phosphate buffer solution (pH 8.0) (Fig. 3b,d). The mixture was stirred for 1 h at 4 °C. After the reaction, 2 mg of dithiothreitol (DTT) was added and the reaction mixture was purified by gel filtration chromatography using a Superdex 200 Increase 10/300 GL column (GE Healthcare). The obtained dimeric protein, dimer **4(Fe-Zn)**, FeP ⊃ N80C–ZnP ⊃ WT, was oxidized by potassium ferricyanide or reduced by DTT and purified again using a HiTrap desalting column (GE Healthcare). The same procedure was used to prepare and characterize dimer **5(Fe-Zn)** and dimer **6(Fe-Zn)**.

2.4. Preparation of cytochrome b_{562} Zn-Fe heterodimers

Reconstituted wild-type Cyt b_{562} with maleimide-linked FeP (m–FeP ⊃ WT, 50 nmol) and reconstituted N80C Cyt b_{562} with ZnP (ZnP ⊃ N80C, 150 nmol) were added to 4 mL of 100 mM phosphate buffer solution (pH 8.0) (Fig. 3c,d). The mixture was stirred for 1 h at 4 °C. After the reaction, 2 mg of DTT was added and the reaction mixture was purified by gel filtration chromatography using a Superdex 200 Increase 10/300 GL column (GE Healthcare). The obtained dimeric protein, dimer **4(Zn-Fe)**, ZnP ⊃ N80C–FeP ⊃ WT, was oxidized by potassium ferricyanide or reduced by DTT and purified again using a HiTrap desalting column (GE Healthcare). The same procedures were used to prepare and characterize dimer **5(Zn-Fe)** and dimer **6(Zn-Fe)**.

2.5. Laser flash photolysis

The nanosecond laser flash photolysis studies were carried out using a Q-switched Nd:YAG laser, which delivers 6-ns pulses at 532 nm. The probe source was a continuous 150-W Xenon arc lamp passed through a monochromator. The protein co-assembly solutions (3–12 μM) in degassed 100 mM phosphate buffer (pH 7.0) were prepared in a glovebox in a 10-mm quartz cell. The protein dimer solutions (~ 3 μM) in degassed 100 mM phosphate buffer (pH 7.0) were also prepared in the glovebox in the 10-mm quartz cell. The temperature was maintained at 20 °C during the laser irradiation. The transient absorption changes for the ZnP triplet excited states in the protein assemblies and heterodimers (^{3}ZnP) were monitored at 460 nm. The transient absorption changes for the ZnP radical cation ($ZnP^{\cdot +}$) and radical anion ($ZnP^{\cdot -}$) in the protein assemblies and heterodimers were monitored at 680 nm and 700 nm, respectively. Signals were detected in transmission using a photomultiplier (Unisoku), and the transient signals were digitized using a Tektronix TDS3012 oscilloscope. Signals were averaged from 128 to 3072 repeated measurements. The data were collected in the 0–100 ms range, and then, transferred to a computer for further data analysis. UV–vis spectra of the protein solutions were measured before and after flash photolysis studies to confirm that the sample remained resistant to significant photodegradation.

2.6. Transient absorption decay analysis

The obtained transient absorption decay data were fitted using

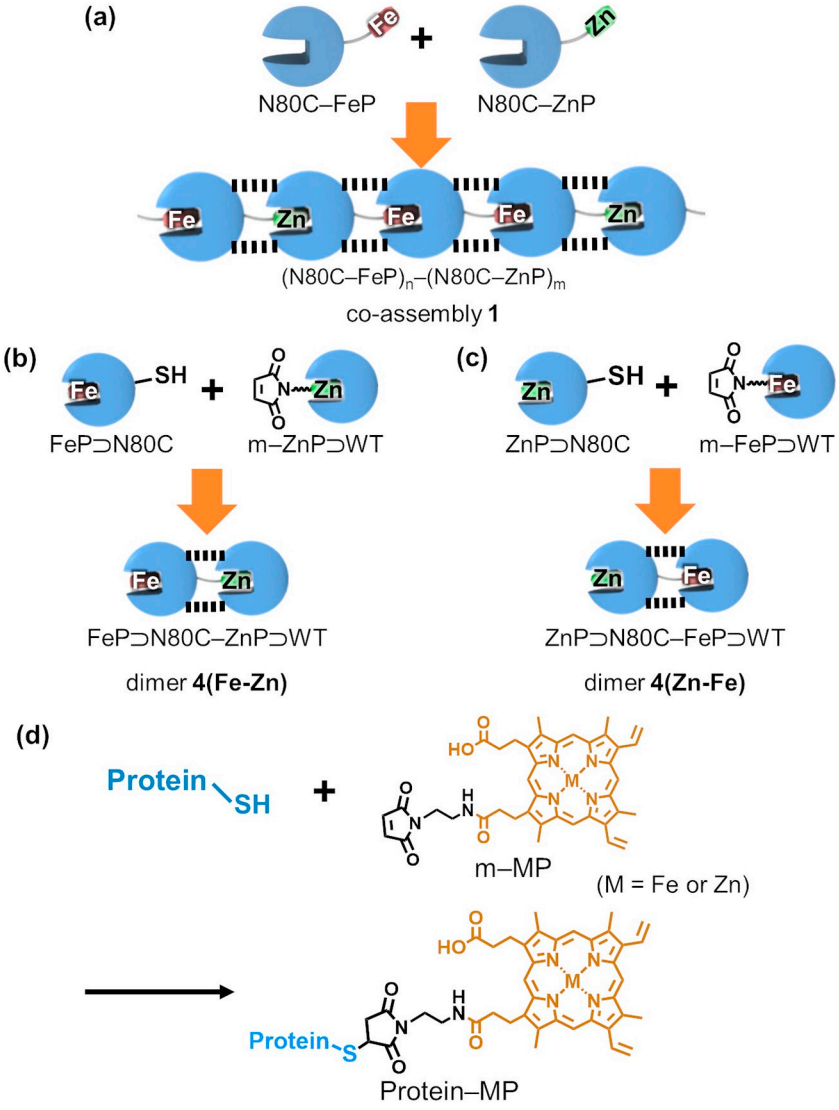

Fig. 3. Preparation methods for (a) co-assembly **1**, (b) dimer **4(Fe-Zn)**, and (c) dimer **4(Zn-Fe)**, and (d) a schematic representation of the reaction between the protein scaffold and the maleimide-linked metalloporphyrin (m–MP: M = Fe or Zn) via maleimide–thiol conjugation.

KaleidaGraph (Version 4.00, Synergy Software). The transient absorption changes of ^{3}ZnP (460 nm) in Cyt b_{562} co-assemblies and heterodimers can be represented by Eq. (1), whereas the ^{3}ZnP decay in non-ET protein oligomers can be fitted using Eq. (2),

$$\Delta\mathrm{Abs} = \alpha e^{-k_a t} + \beta e^{-k_i t} \quad (1)$$

$$\Delta\mathrm{Abs} = \beta e^{-k_i t} \quad (2)$$

where k_i is the kinetic constant of ^{3}ZnP deactivation without ET, and k_a is the sum of the kinetic constant of charge separation (CS: k_{CS}) and k_i.

The transient absorption decay of $ZnP^{\bullet+}$ (680 nm) and $ZnP^{\bullet-}$ (700 nm) can be analyzed by Eq. (3),

$$\Delta\mathrm{Abs} = a_1 e^{-k_a t} + a_2 e^{-k_{CR} t} + a_3 e^{-k_i t} \quad (3)$$

where k_{CR} is the kinetic constant of charge recombination (CR). When k_{CR} is higher than k_a, a_2 has a negative value. On the other hand, assuming that k_a is almost equal to or slightly higher than k_{CR}, a_1 becomes negative (See SI).

3. Results and discussion

3.1. Preparation and characterization of Cyt b_{562} assemblies, co-assemblies, and heterodimers

The Cyt b_{562} assemblies containing ZnP ($(N80C–ZnP)_m$, $(R98A/N80C–ZnP)_m$, and $(D73A/N80C–ZnP)_m$) were prepared in a reaction of N80C with maleimide-linked ZnP on the surface of the protein as shown in Fig. 1. After denaturation by guanidine-HCl, FeP and excess maleimide-linked ZnP were removed by extraction using 2-butanone and the aqueous solution was then neutralized. The obtained protein units were identified by ESI-TOF MS and UV–vis spectra. The CD spectrum of $(N80C–ZnP)_m$ exhibits the split-type Cotton effect in the range of 390–450 nm, which indicates that ZnP has a fixed orientation in the assembly (Fig. S1) [27]. The Cyt b_{562} co-assemblies (co-assemblies **1**, **2**, and **3**) were prepared by mixing the FeP-containing Cyt b_{562} assembly and the ZnP-containing Cyt b_{562} assembly and the changes of the profiles in size exclusion chromatography were reached within 10 h, indicating attainment of equilibrium in the co-assembling events (Figs. 3a and S2). The resultant co-assemblies were identified by UV–vis spectra and size exclusion chromatography (Fig. S2).

The six different Cyt b_{562} heterodimers (Fig. 2b) were also prepared

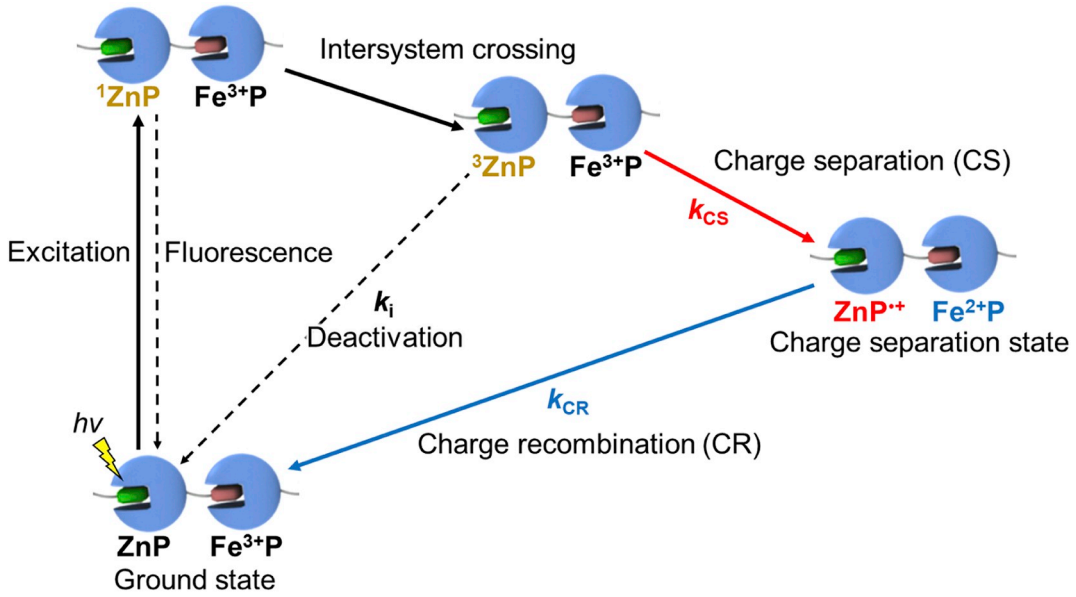

Scheme 1. Photochemical process of oxidative ET in the co-assemblies and heterodimers.

by mixing of two proteins via maleimide–thiol conjugation as shown in Fig. 3b–d, and purified by size exclusion chromatography. The obtained heterodimers were identified by UV–vis spectra and size exclusion chromatography (Fig. S3).

3.2. Evaluation of photoinduced ET in the co-assemblies

Photoinduced ET reactions within the co-assemblies and heterodimers were investigated by observing transient absorption changes after ns-pulse laser flash photolysis. According to previous reports using ET systems containing hemoproteins with Zn and Fe porphyrins, the charge separation (CS) within Cyt b_{562} co-assemblies and heterodimers should occur via the long-lived triplet excited states of ZnP (~10 ms), whereas CS via the singlet excited states is ruled out because of its short lifetime (~1 ns) for their long donor–acceptor distance (29 Å) [3,15]. Thus, the photochemical process after electronic excitation at 532 nm within these co-assemblies and heterodimers is proposed as shown in Scheme 1: (i) photoexcitation to generate the singlet state of the zinc porphyrin species (^{1}ZnP); (ii) intersystem crossing to obtain the long-lived triplet state (^{3}ZnP); (iii) CS between ^{3}ZnP and the ferric species (Fe^{3+}P) in the protein co-assemblies and dimers; and (iv) charge recombination (CR) between the zinc porphyrin radical cation species (ZnP$^{\bullet+}$) and the ferrous species (Fe^{2+}P) in the protein co-assemblies and dimers to recover the ground state (Scheme 1) [15].

First, laser flash photolysis measurements of co-assembly **1**, which has a rigid structure derived from the H-bond interactions at the protein interface were performed. The decay curves of the 460 nm absorption band of ^{3}ZnP, were monitored in co-assemblies having various *n/m* ratios (*n/m* = 1/1, 2/1, 3/1; Figs. 4a and S4) and (N80C–ZnP)$_m$. Biexponential decay curves (eq. 1) were observed for the co-assemblies, whereas the decay for (N80C–ZnP)$_m$ was found to generate a mono-exponential decay curve (eq. 2). These findings indicate that CS occurs within the co-assemblies. The biexponential fitting parameters include two kinetic constants, k_i and k_a: the former is the triplet decay constant without ET and the latter is the sum of the k_i and k_{CS}, a kinetic constant of CS. The obtained kinetic parameters are summarized in Table 1. The slower decays observed in the co-assemblies correspond to the thermal relaxation of ^{3}ZnP in (N80C–ZnP)$_m$ (k_i = 90 ± 3 s^{-1}). The average k_{CS} values of the co-assemblies were determined to be approximately 530 ± 40 s^{-1}. Interestingly, the k_i and k_{CS} values were found to be mostly independent of the *n/m* ratio whereas the populations of decay components depend on the *n/m* ratio - an increase in the *n/m* ratio in the co-assembly provides a larger population of the faster decay component ($\alpha/(\alpha+\beta)$) as shown in Table 1. This finding appears to be reasonable because not all of the N80C–ZnP units in the co-assembly contribute to the ET reactions due to the successive alignment of N80C–ZnP units. Additionally, the N80C–ZnP units with the successive alignments in the co-assembly should statistically decrease with the increase of the ratio of *n/m*.

The kinetic constants of CR in co-assembly **1** were also evaluated by monitoring the transient absorption changes of the ZnP$^{\bullet+}$ species which has a characteristic peak at 680 nm (Figs. 4b and S4). The absorption of the co-assembly **1** at 680 nm after the flash photolysis rapidly increases within 1–2 ms and then undergoes a slow decay. Table 1 shows the summary of kinetic parameters analyzed by Eq. (3). The kinetic constants of CR, k_{CR}, are determined to be 930 ± 50 s^{-1}. Similar to the results inferred from the k_{CS} values, no relationship was observed between the kinetic constants and the *n/m* ratio.

Next, an investigation of transient absorption spectral changes of co-assembly **2** with a semi-rigid structure (vide supra) after the flash photolysis was carried out in the same manner used to investigate co-assembly **1** (Figs. 5a and S5). The kinetic parameters are summarized in Table 2. The averaged values of k_i, k_{CS}, and k_{CR} for the co-assembly were determined to be 88 s^{-1}, 300 s^{-1} and 430 s^{-1}, respectively. The k_{CS} and k_{CR} values of the semi-rigid co-assembly are both smaller than those of the rigid co-assembly, whereas the k_i values are close to each other. These results indicate two important characteristics of co-assembly **2**: the photochemical properties of the ^{3}ZnP of co-assembly **2** are similar to those of co-assembly **1**, whereas slower ET events in CS and CR were observed in co-assembly **2** compared with co-assembly **1**, indicating that the H-bond network in co-assembly **1** could be important for the ET events in terms of the structure and/or the ET pathway. Furthermore, the increase of the *n/m* ratio enhances the population of the faster phasic decay in co-assembly **2**. Although this relationship is similar to the relationship observed for co-assembly **1**, the population of the faster phase in co-assembly **2** is smaller than that in co-assembly **1**. This finding suggests that co-assembly **2** is a mixture of the rigid and flexible structures which are formed by the weakened H-bond network relative to co-assembly **1**.

The transient absorption spectral changes of co-assembly **3** with the flexible structure without the interprotein H-bond network were evaluated. In contrast to the results observed for the co-assemblies **1** and **2**, the decay curve of ^{3}ZnP in co-assembly **3** is fitted by the mono-exponential equation to provide essentially the same kinetic constant as

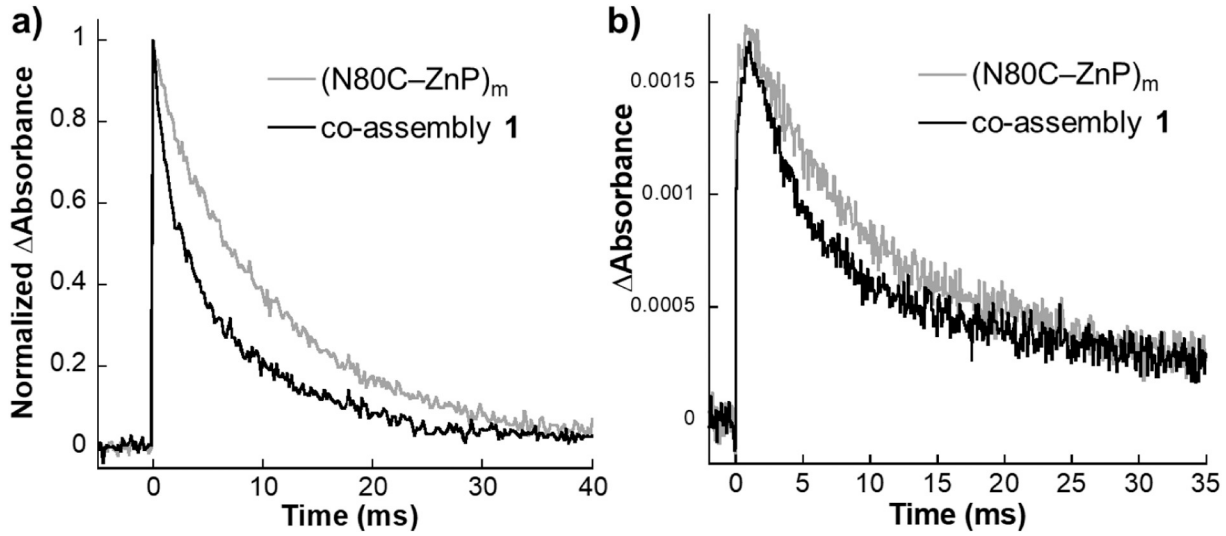

Fig. 4. Transient absorption decays of $(N80C–ZnP)_m$ (gray) and co-assembly **1** (n/m = 3/1, black). (a) Normalized transient absorption decay at 460 nm and (b) transient absorption decay at 680 nm.

Table 1
electron transfer kinetic parameters for co-assembly **1**[a].

n/m	$\frac{\alpha}{\alpha+\beta}$ [b]	$\frac{\beta}{\alpha+\beta}$ [b]	k_{CS} (s^{-1})[b]	k_{CR} (s^{-1})[c]	k_i (s^{-1})[b]
0/1[d]	–	–	–	–	90 ± 3[e]
1/1	0.25 ± 0.02	0.75 ± 0.02	530 ± 62	910 ± 90	81 ± 3
2/1	0.31 ± 0.08	0.69 ± 0.08	510 ± 100	974 ± 120	94 ± 10
3/1	0.44 ± 0.02	0.56 ± 0.02	520 ± 30	913 ± 120	91 ± 4
Average[f]	–	–	530 ± 40	930 ± 50	87 ± 3

[a]Conditions: [N80C–ZnP] = 3 μM and [N80C–FeP] = 0–9 μM in 100 mM phosphate buffer, pH 7.0, at 20 °C under an N_2 atmosphere. [b]Parameters were obtained from Eq. (1). [c]k_{CR} was obtained from Eq. (3). [d]Transient decay of $(N80C–ZnP)_m$. [e]k_i was obtained from Eq. (2). [f]The averaged kinetic constants of co-assembly **1** were calculated using all of the experimental results.

Table 2
Electron Transfer Kinetic Parameters for Co-assembly **2**[a].

n/m	$\frac{\alpha}{\alpha+\beta}$ [b]	$\frac{\beta}{\alpha+\beta}$ [b]	k_{CS} (s^{-1})[b]	k_{CR} (s^{-1})[c]	k_i (s^{-1})[b]
0/1[d]	–	–	–	–	86 ± 5[e]
2/1	0.17 ± 0.03	0.83 ± 0.03	300 ± 260	450 ± 130	86 ± 13
3/1	0.23 ± 0.06	0.77 ± 0.06	310 ± 70	410 ± 20	90 ± 8
average[f]	–	–	300 ± 70	430 ± 40	88 ± 3

[a]Conditions: [R98A/N80C–ZnP] = 3 μM and [R98A/N80C–FeP] = 0–9 μM in 100 mM phosphate buffer, pH 7.0, at 20 °C under an N_2 atmosphere. [b]Parameters were obtained from Eq. (1). [c]k_{CR} was obtained from Eq. (3). [d]Transient decay of $(R98A/N80C–ZnP)_m$. [e]k_i was obtained from Eq. (2). [f]The averaged kinetic constants of co-assembly **2** were calculated using all of the experimental results.

$(N80C–ZnP)_m$ (k_i = 89 ± 1 s^{-1}, Figs. 5a and S6), clearly indicating that CS does not occur in co-assembly **3**. This could be caused by the longer distance between ZnP and FeP for the ET events and/or the lack of the H-bond network in the flexible structure.

Both CS and CR in co-assembly **1** are significantly faster than in the other two co-assemblies. The major differences among these co-assemblies are the strength of the interprotein H-bond network and the related structural rigidity which should provide a shorter ZnP–FeP distance compared with more flexible structures. Thus, these findings emphasize the importance of an interprotein H-bond network in providing a favorable ZnP–FeP distance and/or the pathway for ET in this system.

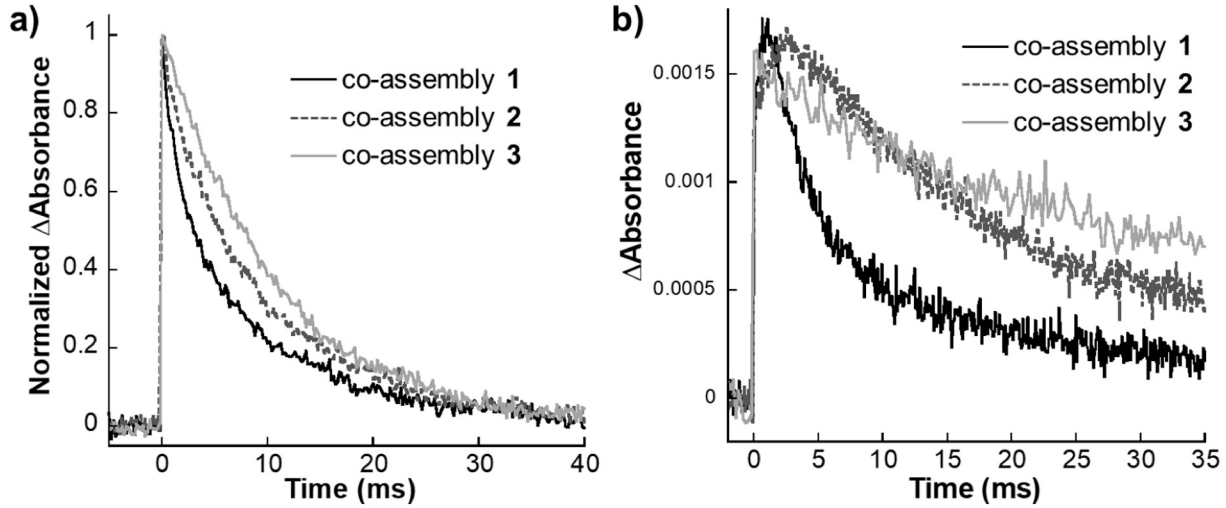

Fig. 5. Transient absorption decays of co-assemblies (black solid line: co-assembly **1**, gray dotted line: co-assembly **2**, gray solid line: co-assembly **3**; n/m = 3/1) at (a) 460 nm and (b) 680 nm.

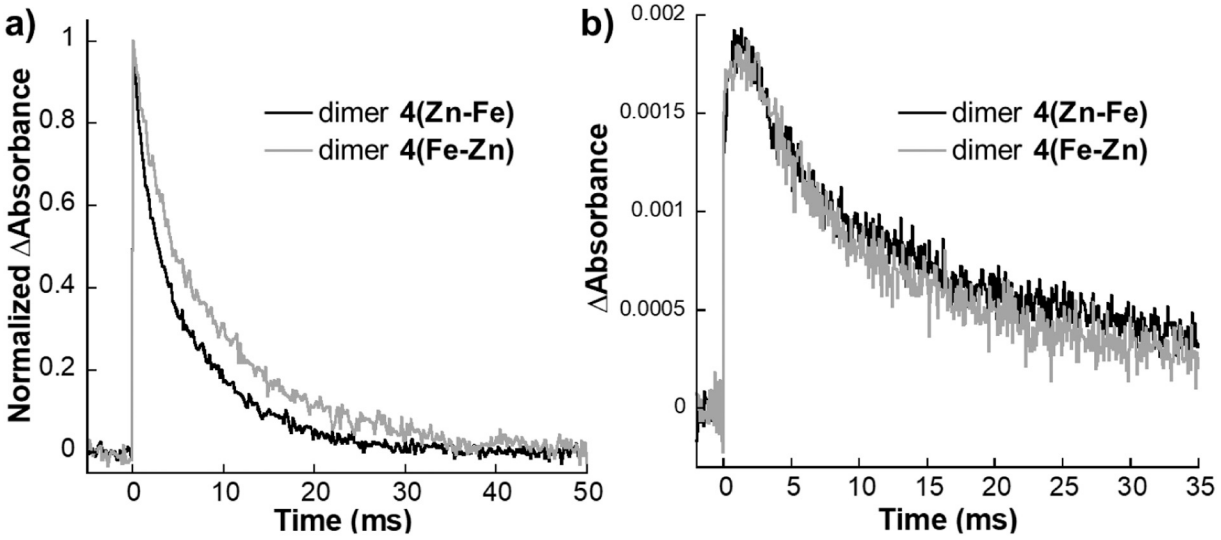

Fig. 6. Transient absorption decays of dimers **4(Zn-Fe)** and **4(Fe-Zn)** (black: dimer **4(Zn-Fe)**, gray: dimer **4(Fe-Zn)**) at (a) 460 nm and (b) 680 nm.

3.3. Evaluation of photoinduced ET in heterodimers

The ET event observed in each co-assembly includes a mixture of reactions with two possible directions as shown in Fig. 2a. Since these characteristics would provide an obscure ET parameter, the exact kinetic parameters with defined directions were determined using six types of Cyt b_{562} heterodimers as shown in Fig. 2b. The transient absorption changes of a series of the heterodimers were monitored and analyzed in the same manner as shown for the co-assembly (Figs. 6, S7, and S8). The kinetic parameters are summarized in Table 3. In the photoinduced ET kinetics for the heterodimers, unignorable populations with k_i values derived from ET-inactive species are unexpectedly observed, indicating that the heterodimers are structurally unstable compared to the co-assemblies. However, it is likely that the ET occurs in the suitable conformation of the heterodimers which have a structure similar to the co-assembly. From the kinetic results, the following three characteristics were identified: (i) the most favorable ET reactions in both CS and CR were observed in the dimer **4(Zn-Fe)** system; (ii) the kinetic parameters of the dimer **4(Fe-Zn)** system clearly indicate slower ET events relative to the dimer **4(Zn-Fe)**; and (iii) the interprotein H-bond network is important for ET events (this observation is consistent with the results observed in the co-assemblies).

It is especially notable that Zn-Fe dimers mediate faster ET than the corresponding Fe-Zn dimers except for the dimers **6(Fe-Zn)** and **6(Zn-Fe)** which do not mediate ET. Also of interest is that the kinetic parameters depend on the ET direction, although both the Zn-Fe and the Fe-Zn dimers are expected to have similar structures. The structural differences are only derived from the positions of ZnP and FeP and the chemical modification of the propionic acid of the protoporphyrin IX ligand. However, the effect of the propionic acid on the redox potential is considered to be negligible to induce this significant change [46]. Thus, the kinetic difference should be caused by the positions of the electron donor and acceptor.

Table 3
Kinetic constants of oxidative ET of heterodimers[a].

	k_{CS} (s^{-1})[b]	k_{CR} (s^{-1})[c]	k_i (s^{-1})[b,f]
dimer **4(Zn-Fe)**	600 ± 30	920 ± 30	120 ± 2
dimer **4(Fe-Zn)**	320 ± 40	580 ± 70	87 ± 2
dimer **5(Zn-Fe)**	370 ± 50	520 ± 20	100 ± 3
dimer **5(Fe-Zn)**	120 ± 10	180 ± 4	78 ± 1
dimer **6(Zn-Fe)**	N.D.[d]	N.D.[d]	100 ± 2[e]
dimer **6(Fe-Zn)**	N.D.[d]	N.D.[d]	80 ± 1[e]

[a]Conditions: About 3 μM of heterodimer in 100 mM phosphate buffer, pH 7.0, at 20 °C under an N_2 atmosphere. [b]Parameters were obtained from Eq. (1). [c]k_{CR} was obtained from Eq. (3). [d]Not-detected. [e]k_i was obtained from Eq. (2). [f]These small differences of k_i values are considered to be caused by the difference of degree of solvation of ZnP or protein-conjugated ZnP in the heterodimers [44,45].

3.4. Reductive ET in dimers 4(Zn-Fe) and 4(Fe-Zn)

The reductive ET events from the viewpoint of Marcus theory (vide infra) in the dimers **4(Fe-Zn)** and **4(Zn-Fe)** were also examined to evaluate the properties of the ET reactions. The reductive quenching of ^{3}ZnP by ferrous FeP (Fe^{2+}P) provides the ZnP radical anion (ZnP$\cdot^-$) as a charge separation species (Scheme 2) [37,47]. The driving force for this ET reaction is completely different from the oxidative ET as shown in Scheme 1. Evaluating the kinetic constants of the reductive ET give important insights into the properties of the ET reaction using Marcus semi-classical theory.

The transient absorption changes of the reduced dimers **4(Fe-Zn)** and **4(Zn-Fe)** were recorded after the flash photolysis. The ^{3}ZnP decays of both dimers **4(Fe-Zn)** and **4(Zn-Fe)** measured at 460 nm follow biexponential kinetics, indicating that the ET reaction proceeds from Fe^{2+}P to ^{3}ZnP (dimer **4(Zn-Fe)**: $k_{CS} = 140 \pm 10\,s^{-1}$, dimer **4(Fe-Zn)**: $k_{CS} = 53 \pm 20\,s^{-1}$, Fig. 7a, Table 4). The charge recombination process of the ET reactions was evaluated using the observed triexponential transient decay at 700 nm (dimer **4(Zn-Fe)**: $k_{CR} = 14 \pm 8\,s^{-1}$, dimer **4(Fe-Zn)**: $k_{CR} = 5 \pm 3\,s^{-1}$, Fig. 7b, Table 4) [47]. Faster CS and CR values were observed in dimer **4(Zn-Fe)** relative to dimer **4(Fe-Zn)** and this result is consistent with the oxidative ET.

3.5. Evaluation of physical properties of ET

According to Marcus semi-classical theory, the kinetic constant of non-adiabatic ET is given by

$$k_{ET} = \sqrt{\frac{\pi}{h^2 \lambda k_B T}} H_{AB}^2 exp\left\{-\frac{(\Delta G^o + \lambda)^2}{4\lambda k_B T}\right\} = k_0 \exp\left\{-\frac{(\Delta G^o + \lambda)^2}{4\lambda k_B T}\right\} \quad (4)$$

where the kinetic constant of ET (k_{ET}) depends on the driving force for ET ($-\Delta G^\circ$), the reorganization energy (λ), and the electronic coupling matrix element (H_{AB}) or k_0 which represents the kinetic constant of ET at $\Delta G^\circ = -\lambda$ [3,7]. Applying the kinetic constants observed in the heterodimers to Eq. (4) confirms whether the major factor for the

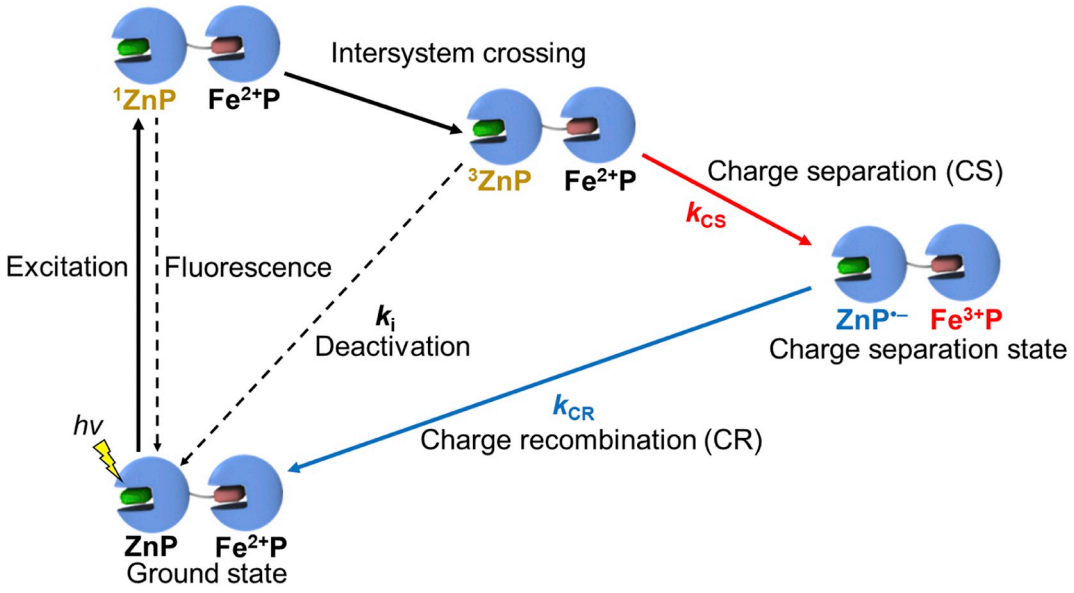

Scheme 2. Photochemical processes of reductive electron transfer in dimers **4(Zn-Fe)** and **4(Fe-Zn)**.

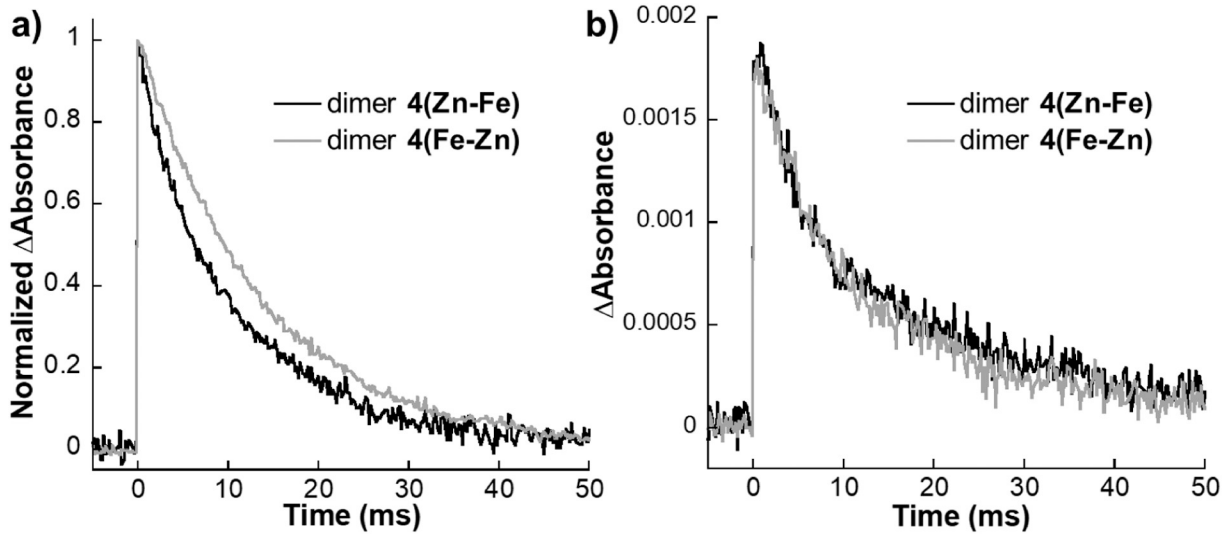

Fig. 7. Transient absorption decays of dimers **4(Zn-Fe)** and **4(Fe-Zn)** during reductive ET reaction (black: dimer **4(Zn-Fe)**, gray: dimer **4(Fe-Zn)**) at (a) 460 nm and (b) 700 nm.

Table 4
Reductive electron transfer kinetics of dimers **4(Zn-Fe)** and **4(Fe-Zn)**[a].

	k_{CS} (s^{-1})[b]	k_{CR} (s^{-1})[c]	k_i (s^{-1})[b]
Dimer **4(Zn-Fe)**	140 ± 10	14 ± 8	78 ± 2
Dimer **4(Fe-Zn)**	53 ± 15	5 ± 3	69 ± 2

[a]Conditions: About 3 μM of reduced heterodimers in 100 mM phosphate buffer, pH 7.0, at 20 °C under an N_2 atmosphere. [b]Parameters were obtained from Eq. (1). [c]k_{CR} was obtained from Eq. (3).

Table 5
Driving forces (−ΔG°) for the oxidative and reductive CSs and CRs for the heterodimers.

	Charge separation, $-\Delta G^\circ$ (eV)	Charge recombination, $-\Delta G^\circ$ (eV)
Oxidative ET	0.97	0.73
Reductive ET	0.33	1.37

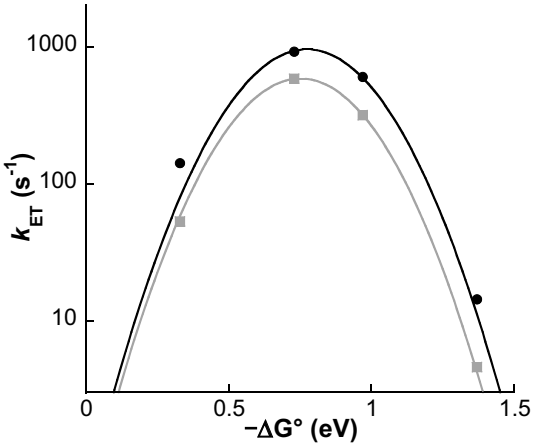

Fig. 8. Driving-force dependence of the ET kinetics in dimers **4(Zn-Fe)** (circle, black) and **4(Fe-Zn)** (square, gray).

Table 6
Parameters of ET Reactions of the Heterodimers Obtained from Eq. (4).

	k_0 (s^{-1})	H_{AB} (cm^{-1})	λ (eV)
Dimer **4(Zn-Fe)**	950 ± 40	1.80×10^{-3}	0.77 ± 0.02
Dimer **4(Fe-Zn)**	580 ± 4	1.40×10^{-3}	0.75 ± 0.01

kinetic difference between dimers **4(Zn-Fe)** and **4(Fe-Zn)** is derived from the electronic coupling matrix element or the reorganization energy.

The driving force of ET was estimated from the redox potentials of each species which appears during the ET reaction (Tables 5, S1 and S2, Scheme S1). The experimental k_{ET} values for CS and CR of the dimers **4(Zn-Fe)** and **4(Fe-Zn)** were plotted as a function of $-\Delta G^{\circ}$ (Fig. 8). The plots were fitted to Eq. (4) using a nonlinear least squares analysis, yielding the values of k_0, H_{AB}, and λ for both dimers **4(Zn-Fe)** and **4(Fe-Zn)** (Table 6). The reorganization energies of both dimers are similar ($\lambda \approx 0.76$ eV) while the H_{AB} and k_0 values are different. These results indicate that the difference between the ET kinetic constant of the Zn-Fe dimer and the ET kinetic constant of the Fe-Zn dimer is not derived from the reorganization energy, but from the electronic coupling matrices of these heterodimers.

Moreover, because Eq. (4) is based on a single-step ET, the close fitting of the ET kinetic constants to Eq. (4) provides evidence for the single-step ET occurring in the heterodimers. Additionally, the redox potentials of the aromatic residues in Cyt b_{562} (Tyr101, Tyr105, Phe61 and Phe65) are much higher than the redox potential of ZnP in the heterodimers (TyrOH$\cdot^+$/TyrOH: $E^0 \geq 1.4$ V [48], Phe$\cdot^+$/Phe: $E^0 \geq 2.0$ V [49], ZnP$\cdot^+$/ZnP: $E^0 \approx 0.9$ V [15,50]) to achieve multistep electron hopping although these residues are located near the heme-binding site. Furthermore, the electron hopping through TyrO$\cdot$/TyrOH ($E^0 = 0.93$ V [51]) is implausible due to the lack of suitable proton acceptor nearby the Tyr residues to decrease the activation barrier of the concerted oxidation and deprotonation [6]. Hence, it is suggested that the single-step ET occurs in the system [52].

4. Conclusion

We demonstrate ET reactions in Cyt b_{562} N80C mutant-based co-assemblies and heterodimers containing Fe and Zn porphyrin moieties. When the plausible Fe—Fe distance (29 Å) estimated in the N80C–FeP assembly is expressed as a donor–acceptor distance in the structurally-defined heterodimers and co-assemblies, long single-step ETs occur in the proteins. The present findings indicate that the interprotein H-bond network is essential for the single-step ET events. The larger kinetic constants of the Zn-Fe dimer relative to those of the Fe-Zn dimer are possibly caused by the slight structural differences. The discussion of these differences including precise pathway should be considered after performing quantum-mechanics level calculations which would provide additional information of the effect of protein structure and residues [53,54]. These findings will give us the new insight not only into the modulation of donor–acceptor distance [3] or reorganization energy of protein [55] but also into the fine-tuning of the protein structure and electron transfer pathway which are effective to control the ET kinetics in hemoprotein. Although the fine-tuning of these factors requires the distinct computational simulation, this strategy will be an effective tool to design an artificial system to replicate the efficient ET in photosynthetic proteins.

Acknowledgment

This work was supported by Grants-in-Aid for Scientific Research provided by JSPS KAKENHI grant numbers JP15H05804, JP15H00873, JP16K14036, JP16H06045 and JP16H00837. We appreciate support from JST PRESTO (JPMJPR15S2) and SICORP.

Appendix A. Supplementary data

Experimental details and characterization data. Supplementary data to this article can be found online at doi:https://doi.org/10.1016/j.jinorgbio.2019.01.001.

References

[1] R. Croce, H. van Amerongen, Nat. Chem. Biol. 10 (2014) 492–501, https://doi.org/10.1038/nchembio.1555.
[2] J.R. Winkler, H.B. Gray, Chem. Rev. 114 (2014) 3369–3380, https://doi.org/10.1021/cr4004715.
[3] H.B. Gray, J.R. Winkler, Q. Rev. Biophys. 36 (2003) 341–372, https://doi.org/10.1017/S0033583503003913.
[4] M. Wikström, V. Sharma, V.R.I. Kaila, J.P. Hosler, G. Hummer, Chem. Rev. 115 (2015) 2196–2221, https://doi.org/10.1021/cr500448t.
[5] S. Yoshikawa, A. Shimada, Chem. Rev. 115 (2015) 1936–1989, https://doi.org/10.1021/cr500266a.
[6] C. Shih, A.K. Museth, M. Abrahamsson, A.M. Blanco-Rodriguez, A.J. Di Bilio, J. Sudhamsu, B.R. Crane, K.L. Ronayne, M. Towrie, A. Vlček Jr., J.H. Richards, J.R. Winkler, H.B. Gray, Science 320 (2008) 1760–1762, https://doi.org/10.1126/science.1158241.
[7] K. Takematsu, H. Williamson, A.M. Blanco-Rodríguez, L. Sokolova, P. Nikolovski, J.T. Kaiser, M. Towrie, I.P. Clark, A. Vlček Jr., J.R. Winkler, H.B. Gray, J. Am. Chem. Soc. 135 (2013) 15515–15525, https://doi.org/10.1021/ja406830d.
[8] A.M. Bogdanov, A. Acharya, A.V. Titelmayer, A.V. Mamontova, K.B. Bravaya, A.B. Kolomeisky, K.A. Lukyanov, A.I. Krylov, J. Am. Chem. Soc. 138 (2016) 4807–4817, https://doi.org/10.1021/jacs.6b00092.
[9] G. Renger, T. Renger, Photosynth. Res. 98 (2008) 53–80, https://doi.org/10.1007/s11120-008-9345-7.
[10] B.R. Crane, A.J. Di Bilio, J.R. Winkler, H.B. Gray, J. Am. Chem. Soc. 123 (2001) 11623–11631, https://doi.org/10.1021/ja0115870.
[11] H.B. Gray, J.R. Winkler, Proc. Natl. Acad. Sci. 102 (2005) 3534–3539, https://doi.org/10.1073/pnas.0408029102.
[12] J.R. Winkler, H.B. Gray, J. Am. Chem. Soc. 136 (2014) 2930–2939, https://doi.org/10.1021/ja500215j.
[13] T. Hayashi, Y. Hitomi, H. Ogoshi, J. Am. Chem. Soc. 120 (1998) 4910–4915, https://doi.org/10.1021/ja9723951.
[14] Y. Hitomi, T. Hayashi, K. Wada, T. Mizutani, Y. Hisaeda, H. Ogoshi, Angew. Chem. Int. Ed. 40 (2001) 1098–1101, https://doi.org/10.1002/1521-3773(20010316)40:6<1098::AID-ANIE10980>3.0.CO;2-G.
[15] F.A. Tezcan, B.R. Crane, J.R. Winkler, H.B. Gray, Proc. Natl. Acad. Sci. 98 (2001) 5002–5006, https://doi.org/10.1073/pnas.081072898.
[16] L. Altamura, C. Horvath, S. Rengaraj, A. Rongier, K. Elouarzaki, C. Gondran, A.L.B. Maçon, C. Vendrely, V. Bouchiat, M. Fontecave, D. Mariolle, P. Rannou, A. Le Goff, N. Duraffourg, M. Holzinger, V. Forge, Nat. Chem. 9 (2017) 157–163, https://doi.org/10.1038/nchem.2616.
[17] P. Xiong, J.M. Nocek, J. Vura-Weis, J.V. Lockard, M.R. Wasielewski, B.M. Hoffman, Science 330 (2011) 1075–1078, https://doi.org/10.1126/science.1197054.
[18] Q. Luo, C. Hou, Y. Bai, R. Wang, J. Liu, Chem. Rev. 116 (2016) 13571–13632, https://doi.org/10.1021/acs.chemrev.6b00228.
[19] Y. Bai, Q. Luo, J. Liu, Chem. Soc. Rev. 45 (2016) 2756–2767, https://doi.org/10.1039/c6cs00004e.
[20] M. Yamanaka, M. Hoshizumi, S. Nagao, R. Nakayama, N. Shibata, Y. Higuchi, S. Hirota, Protein Sci. 26 (2017) 464–474, https://doi.org/10.1002/pro.3090.
[21] W. Zhang, Q. Luo, L. Miao, C. Hou, Y. Bai, Z. Dong, J. Xu, J. Liu, Nanoscale 4 (2012) 5847–5851, https://doi.org/10.1039/c2nr31244a.
[22] S. Biswas, K. Kinbara, T. Niwa, H. Taguchi, N. Ishii, S. Watanabe, K. Miyata, K. Kataoka, T. Aida, Nat. Chem. 5 (2013) 613–620, https://doi.org/10.1038/nchem.1681.
[23] J.D. Brodin, X.I. Ambroggio, C. Tang, K.N. Parent, T.S. Baker, F.A. Tezcan, Nat. Chem. 4 (2012) 375–382, https://doi.org/10.1038/nchem.1290.
[24] K. Oohora, A. Onoda, T. Hayashi, Chem. Commun. 48 (2012) 11714–11726, https://doi.org/10.1039/c2cc36376c.
[25] K. Oohora, T. Hayashi, Curr. Opin. Chem. Biol. 19 (2014) 154–161, https://doi.org/10.1016/j.cbpa.2014.02.014.
[26] K. Oohora, Y. Onuma, Y. Tanaka, A. Onoda, T. Hayashi, Chem. Commun. 53 (2017) 6879–6882, https://doi.org/10.1039/c7cc02678a.
[27] K. Oohora, N. Fujimaki, R. Kajihara, H. Watanabe, T. Uchihashi, T. Hayashi, J. Am. Chem. Soc. 140 (2018) 10145–10148, https://doi.org/10.1021/jacs.8b06690.
[28] H. Kitagishi, Y. Kakikura, H. Yamaguchi, K. Oohora, A. Harada, T. Hayashi, Angew. Chem. Int. Ed. 48 (2009) 1271–1274, https://doi.org/10.1002/anie.200804006.
[29] A. Onoda, Y. Kakikura, T. Uematsu, S. Kuwabata, T. Hayashi, Angew. Chem. Int. Ed. 51 (2012) 2628–2631, https://doi.org/10.1002/anie.201105186.
[30] H. Nikkila, R.B. Gennis, S.G. Sligar, Eur. J. Biochem. 202 (1991) 309–313, https://doi.org/10.1111/j.1432-1033.1991.tb16377.x.
[31] The donor-acceptor distances in the R98A/N80C and D73A/N80C-based co-assemblies and heterodimers are estimated to be variable ranged from 27 Å to 42 Å according to MD simulation results from various initial protein dimer structures [27].
[32] J. Sukegawa, C. Schubert, X. Zhu, H. Tsuji, D.M. Guldi, E. Nakamura, Nat. Chem. 6 (2014) 899–905, https://doi.org/10.1038/nchem.2026.
[33] K. Pettersson, K. Kilså, J. Mårtensson, B. Albinsson, J. Am. Chem. Soc. 126 (2004)

6710–6719, https://doi.org/10.1021/ja0370488.
[34] E. Göransson, J. Boixel, C. Monnereau, E. Blart, Y. Pellegrin, H. Becker, L. Hammarström, F. Odobel, Inorg. Chem. 49 (2010) 9823–9832, https://doi.org/10.1021/ic100605t.
[35] H. Imahori, D.M. Guldi, K. Tamaki, Y. Yoshida, C. Luo, Y. Sakata, S. Fukuzumi, J. Am. Chem. Soc. 123 (2001) 6617–6628, https://doi.org/10.1021/ja004123v.
[36] T.D.M. Bell, K.P. Ghiggino, K.A. Jolliffe, M.G. Ranasinghe, S.J. Langford, M.J. Shephard, M.N. Paddon-Row, J. Phys. Chem. A 106 (2002) 10079–10088, https://doi.org/10.1021/jp014155k.
[37] S.A. Kang, P.J. Marjavaara, B.R. Crane, J. Am. Chem. Soc. 126 (2004) 10836–10837, https://doi.org/10.1021/ja049230u.
[38] N.P. Co, R.M. Young, A.L. Smeigh, M.R. Wasielewski, B.M. Hoffman, J. Am. Chem. Soc. 136 (2014) 12730–12736, https://doi.org/10.1021/ja506388c.
[39] J.L. McGourty, N.V. Blough, B.M. Hoffman, J. Am. Chem. Soc. 105 (1983) 4470–4472, https://doi.org/10.1021/ja00351a056.
[40] T. Koshiyama, M. Shirai, T. Hikage, H. Tabe, K. Tanaka, S. Kitagawa, T. Ueno, Angew. Chem. Int. Ed. 50 (2011) 4849–4852, https://doi.org/10.1002/anie.201008004.
[41] K. Oohora, T. Mashima, K. Ohkubo, S. Fukuzumi, T. Hayashi, Chem. Commun. 51 (2015) 11138–11140, https://doi.org/10.1039/c5cc02680f.
[42] H. Kitagishi, K. Oohora, H. Yamaguchi, H. Sato, T. Matsuo, A. Harada, T. Hayashi, J. Am. Chem. Soc. 129 (2007) 10326–10327, https://doi.org/10.1021/ja073295q.
[43] F.W.J. Teale, Biochim. Biophys. Acta 35 (1959) 543, https://doi.org/10.1016/0006-3002(59)90407-X.
[44] J.E. Kim, M.A. Pribisko, H.B. Gray, J.R. Winkler, Inorg. Chem. 43 (2004) 7953–7960, https://doi.org/10.1021/ic048972.
[45] It is difficult to determine the redox potentials of the dimers **4** due to the dioxygen sensitive nature. Thus, we have considered that the plausible shifts of the redox potential of FeP in the dimers **4** are induced by the change of solvation area. The calculated solvation area of FeP and FeP with the linker in Cyt b_{562} dimer are 154 Å^2 and 132 Å^2, respectively. The redox potential of FeP without linker (dimer **4(Fe-Zn)**) is considered to be same with FeP in wild-type Cyt b_{562}. Although the redox potential of FeP with the linker (dimer **4(Zn-Fe)**) is plausibly changed due to the smaller solvation than FeP, this change will provide small positive shift [56]. Assuming that the redox potential change would be +50 mV, the k_0 value of dimer **4(Zn-Fe)** obtained from Eq. (4) would be $(1.09 \pm 0.07) \times 10^3\ s^{-1}$, which is slightly larger than the case of no redox potantial change (Table 6). Since the k_0 value is still larger than that observed in dimer **4(Fe-Zn)**, the small positive shift of the FeP redox potential is not significant.
[46] K. Harada, M. Makino, H. Sugimoto, S. Hirota, T. Matsuo, Y. Shiro, Y. Hisaeda, T. Hayashi, Biochemistry 46 (2007) 9406–9416, https://doi.org/10.1021/bi7007068.
[47] C. Shen, N.M. Kostić, Inorg. Chem. 35 (1996) 2780–2784, https://doi.org/10.1021/ic9510270.
[48] J.J. Warren, J.R. Winkler, H.B. Gray, FEBS Lett. 586 (2012) 596–602, https://doi.org/10.1016/j.febslet.2011.12.014.
[49] P.B. Merkel, P. Luo, J.P. Dinnocenzo, S. Farid, J. Org. Chem. 74 (2009) 5163–5173, https://doi.org/10.1021/jo9011267.
[50] It is known that the redox potential of Zn porphyrin is not markedly affected by the protein matrix [47]. Therefore, we have applied the redox potential of Zn porphyrin in Cyt *c* as the redox of Zn porphyrin in Cyt b_{562} because the structures including the coordinating amino acid residues are similar.
[51] J.L. Dempsey, J.R. Winkler, H.B. Gray, Chem. Rev. 110 (2010) 7024–7039, https://doi.org/10.1021/cr100182b.
[52] The electron hopping via oxidation of $TyrO^-$ ($TyrO^{\cdot}/TyrO^-$: $E^0 = 0.71$ V [48]) is thermodynamically favorable. However, the pK_a of TyrOH (pK_a = 10.1) is too high to form tyrosinate *in situ*. Thus, this hopping seems to be impossible.
[53] R. Monni, A.A. Haddad, F. van Mourik, G. Auböck, M. Chergui, Proc. Natl. Acad. Sci. 112 (2015) 5602–5606, https://doi.org/10.1073/pnas.1423186112.
[54] C.J. Suess, J.D. Hirst, N.A. Besley, J. Comput. Chem. 38 (2017) 1495–1502, https://doi.org/10.1002/jcc.24793.
[55] O. Farver, N.M. Marshall, S. Wherland, Y. Lu, I. Pecht, Proc. Natl. Acad. Sci. 110 (2013) 10536–10540, https://doi.org/10.1073/pnas.1215081110.
[56] F.A. Tezcan, J.R. Winkler, H.B. Gray, J. Am. Chem. Soc. 120 (1998) 13383–13388, https://doi.org/10.1021/ja982536e.